Optics Letters

Ultrasound detection at fiber end-facets with surface plasmon resonance cavities

Xin Zhou,[1] De Cai,[1] Xiaolong He,[2] Sung-Liang Chen,[1] Xueding Wang,[3] and Tian Yang[1,*]

[1]State Key Laboratory of Advanced Optical Communication Systems and Networks, Key Laboratory for Thin Film and Microfabrication of the Ministry of Education, UM-SJTU Joint Institute, Shanghai Jiao Tong University, Shanghai 200240, China
[2]Xu Yuan Biotechnology Company, 1180 Xingxian Road, Shanghai 201815, China
[3]Department of Biomedical Engineering, University of Michigan, 2200 Bonisteel Blvd., Ann Arbor, Michigan 48109, USA
*Corresponding author: tianyang@sjtu.edu.cn

Received 5 October 2017; revised 6 January 2018; accepted 12 January 2018; posted 12 January 2018 (Doc. ID 308449); published 9 February 2018

Ultrasound detection is performed by measuring laser reflection off a surface plasmon resonance cavity which is integrated at a single-mode fiber end facet. It shows a total noise (or laser RIN) equivalent pressure of 9.7 KPa (or 5.2 KPa) over 0–20 MHz, a 6-dB angular detection range as large as 70° near 10 MHz, a detection bandwidth larger than 125 MHz, and a stable performance for over 20 min without feedback in ambient conditions. Its small form factor, fiber-optic integration, almost omnidirectional responsivity and large bandwidth are favorable for *in vivo* applications and high resolution imaging.

OCIS codes: (240.6680) Surface plasmons; (230.1040) Acousto-optical devices; (060.2370) Fiber optics sensors.

https://doi.org/10.1364/OL.43.000775

Ultrasound sensors with a small size, a flexible configuration, a wide angular response range, and a satisfactory combination of sensitivity and bandwidth are highly desirable for *in vivo* applications. In traditional piezoelectric sensors, improving sensitivity is realized by increasing the size of the sensing element to harvest more acoustic waves. This, in turn, compromises both bandwidth and angular response, because the acoustic vibrations at different locations in the sensing element cancel each other when they are out of phase. Even with normal incidence of acoustic waves, the thickness of the piezoelectric material has to be thinner than half of the acoustic wavelength, which presents a fabrication challenge for high frequency detection. Meanwhile, acousto-optical sensors, which transduce acoustic signals to optical signals, have been reported to achieve high sensitivity, small form factors, and acoustically thin sensing layers. Among them, microring sensors have been studied for the past two decades [1,2]. In 2014, Zhang *et al.* reported a noise equivalent pressure (NEP) as low as 105 Pa and a 350 MHz broad bandwidth using microrings [2]. In the same year, Wang *et al.* reported ultrasound detection using surface plasmon resonance (SPR) for the first time, together with a demonstration of photoacoustic imaging [3]. Their prism coupled SPR, which used water as the sound pressure sensitive material, was reported to have a NEP of 3.3 KPa and a 126 MHz bandwidth. Due to the short depth of the evanescent field of surface plasmon polaritons (SPP), in theory, the prism-coupled SPR has a GHz detection bandwidth for normally incident ultrasound waves [4]. In spite of the high sensitivities and large bandwidths of the above-mentioned acousto-optical microdevices, they have not been presented in convenient and compact configurations for *in vivo* imaging applications. To solve this problem, a valuable solution has been reported by Beard's group, in which a high quality factor (Q) Fabry–Perot (F–P) cavity is fabricated on the end-facet of a single-mode optical fiber (SMF). A NEP of 5 KPa over a 20 MHz measurement bandwidth and a bandwidth of 50 MHz has been reported in 2009 [5]. This kind of sensor has been commercialized and implemented in the UMS3 scanning system of precision acoustics. A kind of tapered sensor has also been reported which has a flatter frequency response with a NEP of 50 KPa [6]. More recently, much higher sensitivities have been reported, with NEP values as low as 8 Pa over 20 MHz [7] and 4 Pa over 5 MHz [8], by creating concave F–P cavities.

In this paper, we report integrating the SPR ultrasound sensor at the SMF end-facet. In this device, SPPs are excited near the end-facet of the SMF core. As the ultrasound signals change the refractive indices and morphologies of the materials that contain the SPPs, the SPR resonance wavelength shift results in a fiber-guided laser reflectivity undulation that follows the sound pressure. The sensing volume has a transverse area comparable to the fiber guided optical mode, and an evanescent depth equal to that of the SPPs. Such a design brings several advantages compared with previous work as follows. First, the ultrasmall sensing volume ensures a large frequency bandwidth and, at the same time, a wide angular range of detection. Second, with the evanescent grating-coupled SPPs as the sensing element, the choice of sensing materials is not limited by what the cavity is made of, as in the cases of microrings and F–P cavities. Neither is the sensing material required to have a lower refractive index than the substrate, as in the prism-coupled SPR or fiber side-wall SPR devices [3]. Third, the relatively lower Q

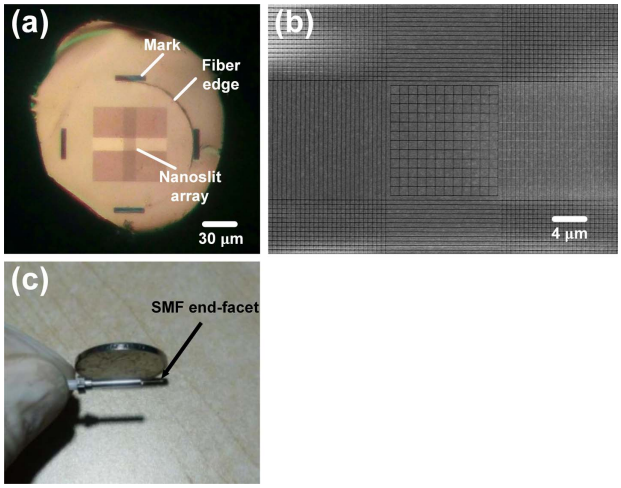

Fig. 1. (a) Optical micrograph of a SMF end-facet which is covered with an SPR cavity aligned to the core of fiber. (b) A scanning electron micrograph of the SPR cavity. (c) The image of a sensor packaged in a fiber-cable ferrule.

of the SPR results in a stable performance, while its sensitivity, in principle, can be made up by using materials with high acousto-optic coefficients.

Figure 1(a) shows the image of our SMF end-facet device under an optical microscope. A 55 nm thick gold film covers the end-facet of the fiber. The circular rim is the edge of the bare fiber, and the four bars are alignment marks. The gold film contains the SPR structure which appears to be square colored shadows in the figure. Figure 1(b) shows the scanning electron micrograph (SEM) of the SPR nanostructure, which is a cavity consisting of 50 nm wide nanoslit arrays which penetrate through the gold film. The nanostructured gold film has been first fabricated on a quartz substrate, then transferred to the SMF end-facet by the glue-and-strip method [9,10]. During the transfer procedure, the fiber-guided broadband reflection spectrum has been monitored in real time by coupling a supercontinuum source into the SMF, to achieve precise alignment between the cavity and the fiber core.

The device design concept and fabrication method inherit our previous work on SMF end-facet biomolecule sensing devices [10,11]. Here, the square-shape nanoslit array in the center has a period of 1020 nm, which couples the fiber guided lightwaves at 1550 nm to SPPs on the inner surface of the gold film, by the grating-coupled SPR effect. By the word inner surface, we refer to the surface between the gold film and the epoxy that glues the gold film to the fiber. By designing the SPPs to reside on the inner surface of the gold film, the sensor is only weakly affected by the refractive index change in the outside environment, to achieve a stable performance for *in vivo* applications. The surrounding nanoslit arrays have a period of 504 nm, forming a distributed reflector (DBR) to confine the SPPs. In certain regions of the DBR, nanoslits of only one direction are contained because the SPPs dominantly propagate in one direction there. The central nanoslit array and the DBR nanoslit array are separated by 500 nm to achieve constructive interference between SPP reflections off the borders of both arrays. Due to the square design, this device is insensitive to the polarization of the fiber guided lightwaves.

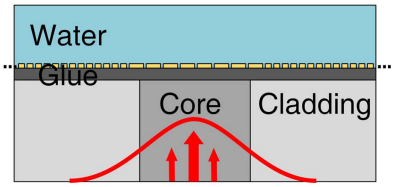

Fig. 2. Schematic of a SPR cavity on top of a 2D waveguide.

Figure 1(c) shows a bare optical fiber packaged in a telecommunication fiber-optic cable ferrule, which contains a ceramic rod and a metallic housing, with the sensor at the fiber end-facet protruding out of the metal housing for about 10 mm. This is the device that we connect to a fiber-optic system for ultrasound detection.

Finite-difference time-domain (FDTD) calculation has been performed to calculate the reflectivity and optimize the geometric parameters of the SPR nanostructure [10]. As illustrated in Fig. 2, a two-dimensional (2D) structure has been used in the simulation. In this 2D model, the fiber is replaced by a 1D dielectric waveguide with a 9 μm wide core, a core refractive index of 1.45, and a cladding refractive index of 1.445. The *p*-polarized waveguide mode is used to excite the SPPs. The gold film and the waveguide are separated by a layer of glue with a nominal thickness of 1 μm. The device is immersed in water. The geometric parameters of the SPR nanoslits are as described in the foregoing. A mesh grid size of 2.5 nm is used inside and near the gold. Perfectly matched layer (PML) boundary conditions are used. Figure 3 shows the SPR resonance dip in the reflection spectrum with different refractive indices of the glue. The calculation results predict a Q of 238, a refractive index sensitivity of 876 nm RIU^{-1}, and a large range of linearity. The glue used in the following experiment has a refractive index of 1.56 according to its product data sheet.

In the following, we characterize the ultrasound detection performance of our SMF end-facet SPR sensor, in terms of NEP, sensitivity, frequency bandwidth, angular response, and time stability. Figure 4(a) shows the experiment setup. The packaged sensor is connected to one end of a SMF. A tunable laser (HP 8186F) is coupled into a SMF and guided by a circulator to reflect off the SPR sensor. The reflected laser light is routed by the same circulator to a photodetector (Menlo FPD310), whose 3-dB band is from 10 to 1000 MHz. The reflected laser power is modulated as the acoustic wave impinges on the sensor and changes its refractive index and

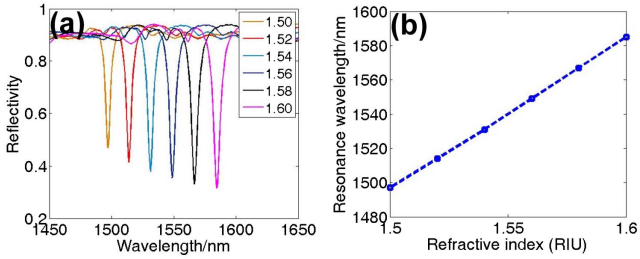

Fig. 3. (a) Calculated reflection spectra with different refractive indices of the glue. (b) The linear relationship between the SPR resonance wavelength and the refractive index of glue.

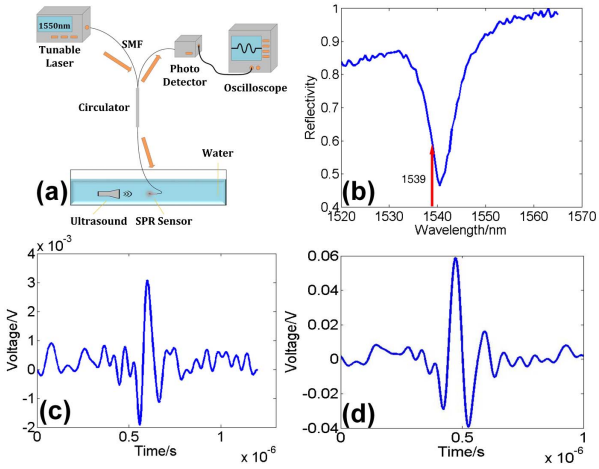

Fig. 4. (a) Experiment setup for acoustic detection. (b) The reflection spectrum of the sensor. (c, d) Oscilloscope readouts of the ultrasound pulses from the same transducer, using (c) our sensor and system and (d) the UMS3 system.

morphology. The photodetector output is recorded by an oscilloscope (LeCroy Wavesurfer 3034) with a 3-dB bandwidth of 350 MHz and a time resolution of 0.5 ns. The ultrasound is generated by either a piezoelectric transducer, or a chromium (Cr) film pumped by a ns-laser, which will be described later.

First, the reflection spectrum of the sensor is acquired by scanning the tunable laser from 1520 to 1565 nm with a wavelength resolution of 0.5 nm, and recording the reflected laser power with a power meter, as plotted in Fig. 4(b). The SPR dip shows a Q of 282, and a depth of approximately 45% compared to nonresonant reflection.

To characterize the sensor's NEP and sensitivity for ultrasound detection, an unfocused transducer (Olympus V312-SU) is used to generate ultrasound pulses with a central frequency of 10 MHz, which is driven by an ultrasonic pulser-receiver (Olympus 5073PR) with an electric pulse energy of 4 μJ. The laser wavelength is set at 1539 nm which corresponds to a large reflectivity-versus-wavelength slope in Fig. 4(b) and a relatively small reflectivity, and the laser power before the photodetector is 1.6 mW. The oscilloscope readout is plotted in Fig. 4(c), after being mathematically filtered by a 20 MHz square low-pass filter. At the same time, the UMS3 scanning system of Precision Acoustics has been used to calibrate the ultrasound pulses from the same transducer, as shown in Fig. 4(d), after being filtered by a 20 MHz square low-pass filter as well. The peak acoustic pressure is measured as 95 KPa. The NEP of the UMS3 measurement results is 5.2 KPa, as obtained from its root-mean-square (RMS) background noise, which agrees well with the reported value in Ref. [5]. Comparing with Fig. 4(c) which shows a peak signal-to-noise ratio (SNR) of 9.8, an NEP of 9.7 KPa over 0–20 MHz is obtained for the measurement results using our sensor and system. Here, the background noises of the measurements are the same as the floors of Figs. 4(c) and 4(d), respectively. Further, after subtracting the noise arising from our electrical system, which is considerably large due to the lack of electrical signal amplification, our sensor is predicted to have a RIN-noise-limited NEP of 5.2 KPa. The subtracted electrical noise has been obtained by turning off the laser and doing the measurement. Further, considering the fact the central frequency of the ultrasound pulses, which is 10 MHz, is the 3-dB frequency of the photodetector; our measurement is expected to be more sensitive and have a lower NEP at higher frequencies.

By performing a Fourier Transform of the oscilloscope readout, we obtain a sensitivity of 718 and 21 mV/MPa at 10 MHz for the UMS3 system and our measurement, respectively. The sensitivity of the latter can be increased by using a photodetector with a higher electrical gain, for example, to over 500 mV/MPa by using Newfocus 1811 in theory. Taking the acousto-optical coefficient of the glue to be 3.7×10^{-4} MPa^{-1}, which is calculated from its refractive index of 1.56 and Young's modulus of 2×10^5 psi according to the product data sheet and the theory in Ref. [12], and assuming that the sound pressure near the sensor surface is equal to that of the ultrasound source, our sensor should have a five times higher sensitivity in theory than the experiment results. This discrepancy may result from the thickness of the glue being thinner than that of the SPP evanescent depth, the glue's acousto-optical coefficient not being calculated accurately, and/or the diffraction and reflection of ultrasound at the fiber tip, which needs further investigation.

To characterize the sensor's frequency response and bandwidth, a broad band ultrasound signal is generated by pumping a 200 nm thick Cr film on a quartz substrate with a pulsed laser at 532 nm, with a pulse width of approximately 5 ns, a repetition rate of 10 Hz, and a focal spot size of 5 mm. The pulsed laser, the quartz/Cr sample, and the sensor are positioned in line. According to the time delay between the laser pulse and the ultrasound signal detected, the distance between the sensor and the Cr film is determined to be 0.5 mm. A photodetector (Newfocus 1801) which has a 3-dB band from 25 KHz to 125 MHz, and which is connected to a 62.5 μm core diameter multimode fiber, is used to measure the profile of the excitation laser, as shown by the blue curve in Fig. 5(a). An ultrasound signal that duplicates the time-domain profile of the laser is expected [2]. The oscilloscope readout from the sensor is also plotted in Fig. 5(a) after 64 times averaging, as a red curve. Here, the reflected laser light is received by a photodetector (Newfocus 1811) whose 3-dB band is from 25 KHz to 125 MHz. The measurement results clearly show that our sensor is able to follow the fast rise and fall of the ultrasound signal. A tail in the sensor response after the ultrasound signal diminishes implicates a relaxation process either in the quartz/Cr sample or the receiving end which needs future investigation. In Fig. 5(b), the Fourier Transform of both the laser profile and the sensor response are plotted, taking only the rising side of the

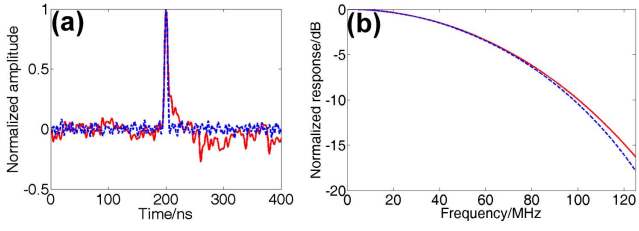

Fig. 5. (a) Blue: excitation laser pulse time-domain profile. Red: sensor response to laser excited ultrasound pulses. (b) Spectra of the sharp pulses in (a), in which the sensor response has been compensated for ultrasound attenuation in water. Here, the definition of dB values is $20\,\mathrm{Log}_{10}$.

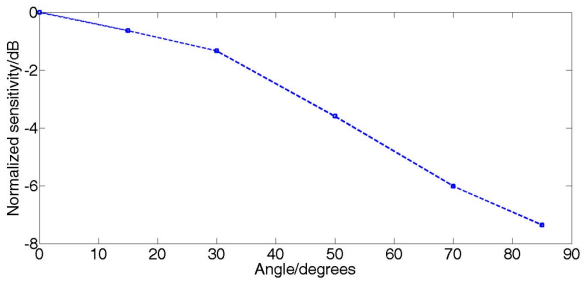

Fig. 6. Sensor's angular response to ultrasound centered around 10 MHz. Here, the definition of dB values is $20\,\mathrm{Log}_{10}$.

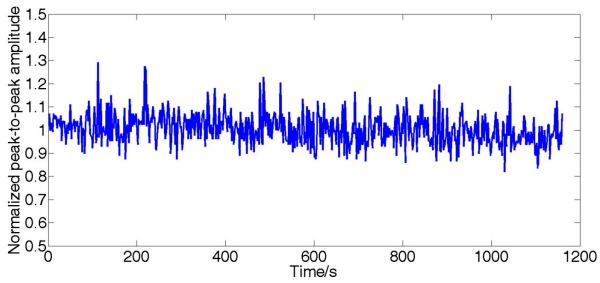

Fig. 7. Oscilloscope readout in ambient conditions for 20 min.

pulse into consideration. The sensor response curve has been compensated for ultrasound attenuation in water, which is taken to be 2×10^{-4} dBmm^{-1} MHz^{-2} [13]. Two factors could make the predicted bandwidth of the ultrasound signal even larger than that of the pulsed laser as in Fig. 5(b), including over-compensation of acoustic attenuation, and the laser pulses being shorter than that measured in Fig. 5(a) due to modal dispersion in the fiber that connects the pulsed laser to the photodetector. We conclude that the sensor has a frequency bandwidth for ultrasound detection of more than 125 MHz, which is limited by the photodetector.

To characterize the sensor's angular response, the same 10 MHz-centered unfocused transducer is used to produce the ultrasound. The measurement result is plotted in Fig. 6. A 6-dB angle as wide as 70° and an almost omnidirectional detection is obtained. The nonuniform angular dependence indicates the anisotropic response of the SPR device to sound pressure, while the acoustic wavelength at 10 MHz is over an order of magnitude larger than the device dimensions and has an ignorable effect on the angular response.

At last, the 10 MHz-centered ultrasound detection experiment has been continuously run for approximately 20 min, with the peak-to-peak readout value of one pulse taken once per *s*, as plotted in Fig. 7. A 6% standard deviation is observed under ambient conditions without any feedback control, showing much better stability than previous work on high-Q sensors.

In summary, we have designed, fabricated, and characterized SPR cavities on SMF end-facets for ultrasound detection. This kind of device shows distinct advantages compared with piezoelectric and other types of optical sensors. Thanks to the ultrasmall sensing volume, it has a large bandwidth of over 125 MHz, and a wide angular range of detection which is 70° at approximately 10 MHz. A total NEP of 9.7 KPa and a RIN-limited NEP of 5.2 KPa over 20 MHz have been obtained, which is comparable to commercial fiber-end F-P cavity sensors. At the same time, the grating-coupled surface wave sensing configuration renders the potential to achieve very high sensitivities with Qs as low as a few hundred in future work, by employing materials that are highly responsive to sound pressure to cover the sensing surface, such as rubber materials with two orders of magnitude lower Young's moduli than the currently used glue, and acoustic metamaterials. In addition, the intermediate Q values make the sensing performance much more stable without feedback control and reproducible between different devices, compared with the ultrahigh Q devices in previous reports. At last, the combination of all of the above merits, i.e., the potential high sensitivity, the large bandwidth, the almost omnidirectional detection and the performance stability, on the tiny end-facet of a SMF, presents a promising candidate for high-resolution phased-array *in vivo* ultrasound imaging in an unprecedented manner.

Funding. National Natural Science Foundation of China (NSFC) (61275168; 11574207); National High Technology R&D Program of China (2015AA020944); Xu Yuan Biotechnology Co.

Acknowledgment. We thank Prof. Aili Zhang and Ying Xin from the Laboratory of Bioheat and Mass transfer, Shanghai Jiao Tong University, and Prof. Qian Cheng, Hao Chen and Yudi Chen from Institute of Acoustics, Tongji University for the use of their equipments and technical assistance. Nanostructure fabrication is done at the Center for Advanced Electronic Materials and Devices of Shanghai Jiao Tong University.

REFERENCES

1. S. Ashkenazi, C. Y. Chao, L. J. Guo, and M. O'donnell, Appl. Phys. Lett. **85**, 5418 (2004).
2. C. Zhang, T. Ling, S. L. Chen, and L. J. Guo, ACS Photon. **1**, 1093 (2014).
3. T. X. Wang, R. Cao, B. Ning, A. J. Dixon, J. A. Hossack, A. L. Klibanov, Q. Zhou, A. Wang, and S. Hu, Appl. Phys. Lett. **107**, 153702 (2015).
4. R. Nuster, G. Paltauf, and P. Burgholzer, Opt. Express **15**, 6087 (2007).
5. P. Morris, A. Hurrell, A. Shaw, E. Zhang, and P. C. Beard, J. Acoust. Soc. Am. **125**, 3611 (2009).
6. P. Morris, A. Hurrell, and P. C. Beard, "Development of a 50 MHz Fabry–Perot type fibre-optic hydrophone for the characterisation of medical ultrasound fields," in *Proceedings of Institute of Acoustics*, St. Albans, Vermont, 2006, pp. 717–725.
7. E. Z. Zhang and P. C. Beard, Proc. SPIE **7899**, 78991F (2011).
8. J. A. Guggenheim, E. Z. Zhang, and P. C. Beard, Proc. SPIE **9708**, 97082M (2016).
9. X. L. He, J. Long, H. Yi, L. Chen, Y. H. Tang, and T. Yang, "Transferring planar surface plasmon resonance structures onto fiber end facets and integration with microfluidics," in *Frontiers in Optics Technical Digest*, Orlando, Florida, 2013, paper FTu1B. 1.
10. X. L. He, H. Yi, J. Long, X. Zhou, J. Yang, and T. Yang, Appl. Phys. Lett. **108**, 231105 (2016).
11. Z. Y. Lei, X. Zhou, J. Yang, X. L. He, Y. L. Wang, and T. Yang, Appl. Phys. Lett. **110**, 171107 (2017).
12. R. D. Alcock and D. C. Emmony, J. Appl. Phys. **92**, 1630 (2002).
13. G. R. Lockwood, D. H. Turnbull, and F. S. Foster, IEEE Trans. Ultrason. Ferroelectr. **41**, 231 (1994).